INORGANIC CHEMISTRY FRONTIERS

RESEARCH ARTICLE

View Article Online
View Journal

Cite this: DOI: 10.1039/d5qi00813a

Coinage metal(I) clusters based on a flexible P,P′(N,N′)$_2$-ligand: colorful phosphorescence, abnormal thermal quenching behavior and anticounterfeiting application†

Andrey Yu. Baranov,[a] Evgeniya P. Doronina,[b] Mariana I. Rakhmanova,[a] Irina Yu. Bagryanskaya,[c] Konstantin A. Brylev,[a] Taisiya S. Sukhikh[a] and Alexander V. Artem'ev*[a]

Unprecedented Cu^{I}, Ag^{I} and Au^{I} clusters with pronounced metallophilic Au–X (X = Cu, Ag, Au) or Ag–Ag contacts have been assembled using 1,2-bis[bis(pyridin-2-ylmethyl)phosphino]ethane (**L**), an innovative P,P′(N,N′)$_2$-ligand. Its interaction with AuCl/KPF$_6$, AuI or (AuC≡CPh)$_n$ yields complexes of the type $[Au_2L_2]^{2+}$, $[Au_2I_2L_2]$ and $[Au_2(C{\equiv}CPh)_2L]_x$ (x = 2 or n), respectively. The reaction of **L** with AgPF$_6$ affords a $[Ag_4L_2]^{4+}$ cluster, while the treatment with AgNO$_3$ leads to a nine-nuclear $[Ag_9L_3(NO_3)_3]^{6+}$ cluster. The latter was transformed into a heterometallic $[Au_2Ag_4L_2(NO_3)_2(H_2O)]^{4+}$ cluster by treatment with [Au(tht)Cl]. Sequential reaction of **L** with Au(I) halides and $[Cu(MeCN)_4]PF_6$ provides heterometallic $[Au_2Cu_4(\mu_2\text{-}Cl)_2L_2]^{4+}$ and $[Au_2Cu_4L_2I_2(MeCN)_4]^{4+}$ ensembles. Most of the title clusters exhibit a charge transfer photoluminescence in the green to orange region with the quantum efficiencies up to an impressive 77%. Surprisingly, the $[Au_2Cu_4L_2I_2(MeCN)_4]^{4+}$ cluster shows an abnormal (negative) thermal quenching of the luminescence, which is unprecedented for Au(I) derivatives. The practical utility of the designed clusters was demonstrated by their application as innovative vapor-responsive emission inks for advanced anticounterfeiting.

Received 19th March 2025,
Accepted 13th June 2025

DOI: 10.1039/d5qi00813a

rsc.li/frontiers-inorganic

Introduction

Currently, ligand-protected Cu^{I}, Ag^{I} and Au^{I} clusters are attracting worldwide attention due to their remarkable structure as well as interesting photophysical, catalytic and biological properties.[1–7] These clusters often exhibit multiple M^{I}···M^{I} interactions, which, together with the ligand structure, significantly affect both the cluster architecture and emission properties.[8–13] Another hallmark of the coinage metal(I) clusters is efficient phosphorescence making them promising emitters for OLED devices,[14–17] X-ray scintillators,[18,19] optical sensors,[20] photocatalysts,[21] anticounterfeiting dyes,[22] and smart materials.[23–26] From an application perspective, heterometallic Au^{I}–Ag^{I}, Au^{I}–Cu^{I}, and Ag^{I}–Cu^{I} clusters are particularly promising because their phosphorescence can be tuned both by tailoring a ligand structure and changing the M/M′ ratio.[27–31]

Among a plethora of the protecting ligands used, pyridylphosphines are enormously important in the chemistry of coinage metal(I) clusters.[32,33] The simultaneous presence of phosphorus and nitrogen atoms makes pyridylphosphines a versatile platform for assembly of the most diverse clusters exhibiting bright phosphorescence[34] or thermally activated delayed fluorescence (TADF).[35–37] Thus, based on the "rigid" (2-Py)$_n$(Ph)$_{3-n}$P (n = 1–3) ligands with direct phosphorus-pyridine linkages, a variety of heterometallic clusters were designed, *e.g.* AuCu$_4$,[38] Au$_2$Cu,[39–41] Au$_2$Cu$_6$,[42] Au$_6$Ag$_7$,[43] Au$_{10}$Ag$_2$,[44] Au$_{13}$Cu$_n$ (n = 2, 4, 8),[45] C@Au$_6$Cu$_2$,[46] and C@Au$_6$Ag$_2$ [47] and C@Au$_6$Ag$_6$.[48] The phosphines with flexible (CH$_2$)$_n$Py arms (n = 1 or 2), while being much less studied, allow the design of fundamentally new clusters with remarkable phosphorescent properties.[34,49–56] For example, (2-PyCH$_2$)$_3$P forms triangular AuAg$_3$ clusters showing rare violet phosphorescence with photoluminescence quantum yields (PLQYs) up to 96%.[51] Meanwhile, pyridyl-substituted

[a]*Nikolaev Institute of Inorganic Chemistry, SB RAS, 3, Lavrentiev Ave., Novosibirsk 630090, Russia. E-mail: chemisufarm@yandex.ru*
[b]*A. E. Favorsky Irkutsk Institute of Chemistry, SB RAS, 1 Favorsky Str., 664033 Irkutsk, Russia*
[c]*N. N. Vorozhtsov Novosibirsk Institute of Organic Chemistry, SB RAS, 9, Acad. Lavrentiev Ave., 630090 Novosibirsk, Russia*

†Electronic supplementary information (ESI) available: General information, copies of the experimental spectra, computation details. CCDC 2420289–2420292, 2265012–2265015 and 2292654. For ESI and crystallographic data in CIF or other electronic format see DOI: https://doi.org/10.1039/d5qi00813a

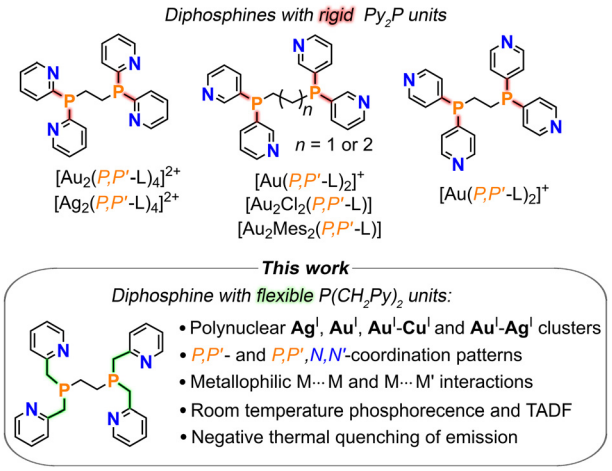

Scheme 1 Overview of known pyridyl-diphosphines and complexes thereof[57–61] as well as key aspects of this study.

diphosphines are very rare and poorly explored, despite their great potential for designing heterometallic clusters with essentially new structures and properties. In particular, the diphosphines shown in Scheme 1 have only sporadically been used for assembly of simple mono- or dinuclear Au(I) or Ag(I) complexes.[57–61] Among the related ligands, pyridyl-substituted 1,5-diaza-3,7-diphosphacyclooctanes can be highlighted as efficient ligands for the luminescent Au_2, Cu_6 and Au_2Cu_4 clusters.[50,62–64]

Herein, we have designed a family of unprecedented homo- and heterometallic Cu(I), Ag(I) and Au(I) clusters supported by 1,2-bis[bis(pyridin-2-ylmethyl)phosphino]ethane, an innovative flexible P,P′(N,N′)$_2$-ligand (Scheme 1). Fortunately, the obtained clusters exhibited fascinating luminescent properties, including bright phosphorescence, abnormal thermal quenching, and non-trivial vapor-sensitive emission behavior.

Results and discussion

Synthetic aspects

We have found that the interaction of **L** with the Au(tht)Cl/KPF_6 system gives the cationic complex $[Au_2L_2](PF_6)_2$ (**1**) (Scheme 2), while the treatment with AuI produces the neutral adduct $[Au_2L_2I_2]$ (**2**). The gold(I) phenylacetylide reacts with **L** to give only adduct $[Au_2(C{\equiv}CPh)_2L]$ (**3**), even at a PhC≡CAu/L molar ratio of 1 : 1. The recrystallization of **3** from a CH_2Cl_2–EtOH mixture yields the crystals of dimer $[Au_2(C{\equiv}CPh)_2L]_2$ (**3a**, major product) and chain polymer $[Au_2(C{\equiv}CPh)_2L]_n$ (**3b**). Much more interesting results were obtained in the reactions with Ag(I) salts. The treatment of **L** with $AgPF_6$ leads to the formation of the four-nuclear cluster $[Ag_4L_2](PF_6)_4$ (**4**), while $AgNO_3$ produces the nine-nuclear cluster $[Ag_9L_3(NO_3)_3](NO_3)_6$ (**5**). For comparison, the related diphosphine, 1,2-bis(di-2-pyridylphosphino)ethane (d2pype), reacts with $AgNO_3$ to give dinuclear complex $[Ag_2(d2pype)_4](NO_3)_2$.[58] Given that the Au^I–Ag^I clusters exhibit much stronger emission than their iso-

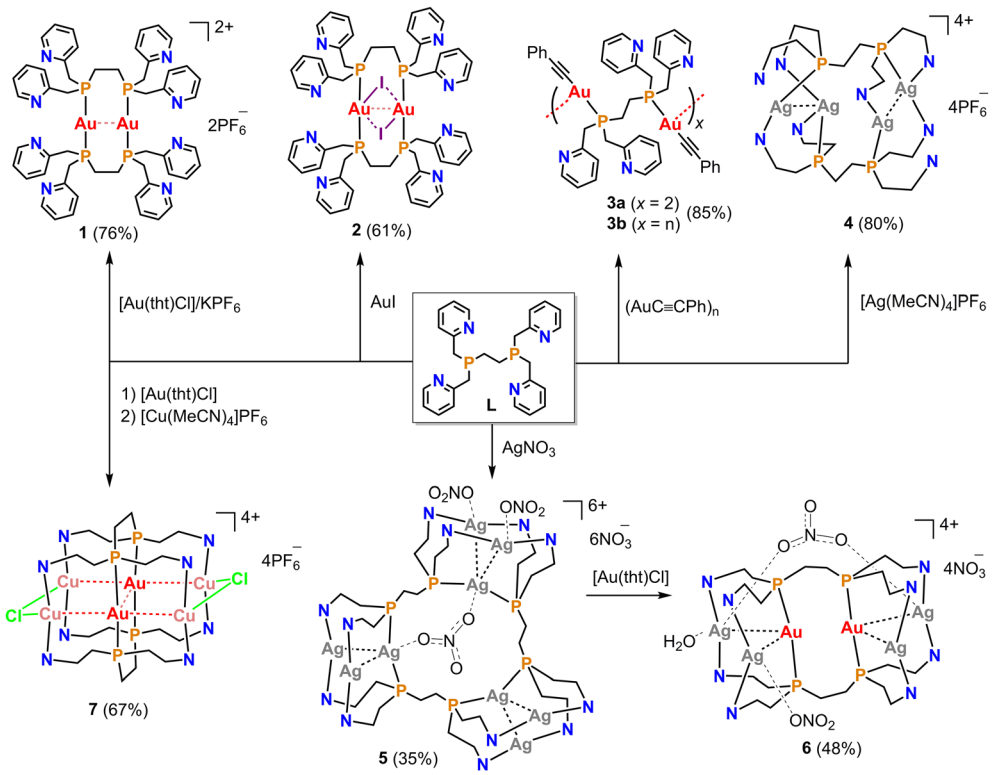

Scheme 2 Synthesis of clusters **1**–**7**.

structural all-Ag analogues,[29,51] we next attempted to replace the P-coordinated Ag(I) ions of **4** on the Au(I) ions by reacting with [Au(tht)Cl]. However, instead of the anticipated product $[Ag_6Au_3L_3](NO_3)_9$, the cluster $[Au_2Ag_4L_2(NO_3)_2(H_2O)](NO_3)_4$ (**6**) was unexpectedly isolated (Scheme 2). Encouraged by these results, we have further exploited the ligand **L** as a platform for stabilizing unprecedented cluster units. Thus, by the interaction of **L** with [Au(tht)Cl] followed by the treatment with $[Cu(MeCN)_4]PF_6$ leads to another heterometallic ensemble $[Au_2Cu_4L_2Cl_2](PF_6)_4$ (**7**) bearing a unique Au_2Cu_4 kernel. Apparently, the assembly of **7** occurs *via* an initial formation of $[Au_2L_2]Cl_2$, whose structure is similar to that of **1** and the related complexes,[65,66] and the further reaction with $[Cu(MeCN)_4]PF_6$ leads to the insertion of Cu^+ ions into CH_2Py arms of $[Au_2L_2]Cl_2$.

In the next step, we attempted to assemble the iodide analog of **7** by treating **2** with $[Cu(MeCN)_4]PF_6$. Again, contrary to our expectations, the unexpected complex $[Au_2Cu_4L_2I_2(MeCN)_4](PF_6)_4$ (**8**) was isolated, in which the Au_2Cu_2 kernel and two MeCN-ligated Cu(I) ions are spaced apart (Scheme 3). Attempts to assemble heterometallic complexes by treating **1** or **3** with Cu^+ or Ag^+ salts were unsuccessful. It should be emphasized that clusters **4–8** are unprecedented, since only the ligand **L** is able to stabilize such ensembles. Obviously, the pseudo-symmetric structure of the complexes **1–8** is due to the symmetric nature of the ligand **L**.

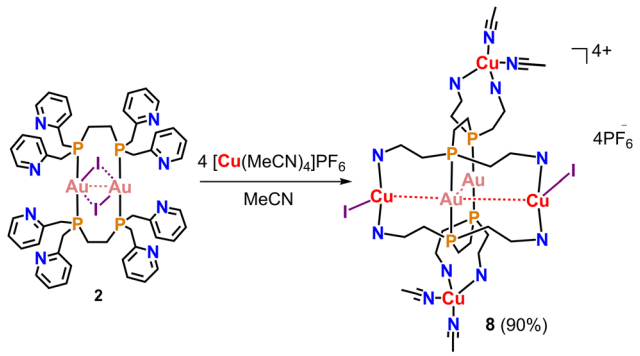

Scheme 3 Synthesis of cluster **8**.

Structural & spectral characterization

Complexes **1**, **2** and **3b** were structurally characterized by X-ray diffraction analysis (XRD) as themselves, while **4–8** and **3a** were characterized as solvates **3a**·EtOH, **4**·2Me_2CO, **5**·8H_2O, **6**·2H_2O, **7**·4Me_2CO·2EtOH and **8**·10MeCN. The X-ray derived structures of Au(I) complexes **1–3** are shown in Fig. 1 (for more information, see Fig. S1–9, ESI†). The cation of **1** is composed of two Au(I) ions P,P′-bridged by two **L** ligands. Both Au(I) ions have a slightly distorted linear Au@P_2 coordination with the P–Au–P angle of ~174–176°. Since the Au–Au intramolecular distance of 2.945 Å is significantly shorter than the sum of van der Waals radii ($\sum r_{vdW(Au-Au)}$ = 3.32 Å),[67] aurophilic interactions can be proposed in **1**. The asymmetric unit of **2** contains two halves of two independent molecules (one of which is shown in Fig. 1) that differ in geometric parameters (Fig. S2†). Like to **1**, each Au(I) ion of **2** is coordinated by two P atoms (∠P–Au–P ≈ 159.2°), and the intramolecular Au–Au distances of 3.069 Å and 3.133 Å also imply aurophilicity. In both independent molecules of **2**, the Au–I distances are longer than the sum of covalent radii (2.75 Å), but shorter than the sum of van der Waals radii ($\sum r_{vdW(Au-I)}$ of 3.64 Å).[67] Herewith, one molecule of **2** contains μ_2-I atoms ($d_{Au-I} \approx 3.272 \pm 0.071$ Å),

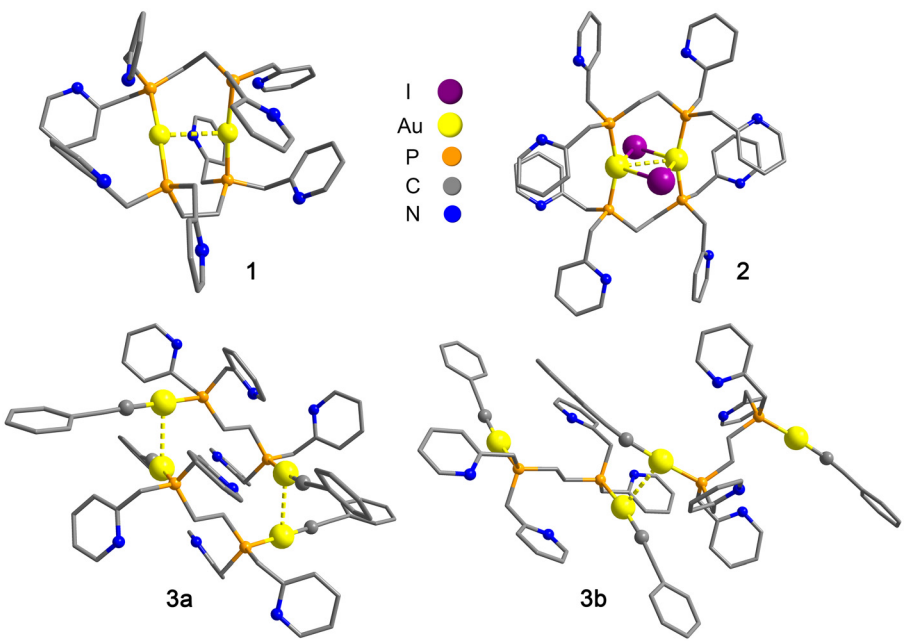

Fig. 1 X-Ray derived structures of Au(I) clusters **1–3**. The H atoms, counterions and solvate molecules are omitted for clarity.

while in another molecule, each iodide is clearly ligated to one Au atom (d_{Au-I} = 3.236 Å), and only associated with the second (d_{Au-I} = 3.574 Å). As mentioned above, complex **3** was isolated as supramolecular dimer (**3a**) and polymer (**3b**) forms, which have a similar molecular structure. In their basic $[Au_2L_2(C{\equiv}CPh)_2]$ fragment, the Au atoms adopt a distorted linear coordination (∠C–Au–P ≈ 175°) with Au–P and Au–C bonds being comparable to the literature values for related complexes. In the dimer **3a**, the $[Au_2L_2(C_2Ph)_2]$ molecules are dimerized *via* intermolecular Au···Au metallophilic contacts of 3.072 Å (92% $\sum r_{vdW(Au-Au)}$).[67] In contrast, in the packing of **3b**, the $[Au_2L_2(C_2Ph)_2]$ molecules form 1D supramolecular chains through intermolecular Au–Au contacts of 3.203 Å (96% $\sum r_{vdW(Au-Au)}$).[67] To our knowledge, it is the first example of aurophilicity-bonded 1D polymers based on the $[Au(C{\equiv}CR)_2L]$ molecules (L is a diphosphine). The related complexes, $[Au(C{\equiv}CR)_2(dppe)]$ and $[Au(C{\equiv}CR)_2(dppp)]$, like **3a**, are all Au–Au bonded dimers.[68–70]

The molecular structures of **4–8** are shown in Fig. 2. The cation of **4** consists of two **L** molecules and four Ag^+ ions, each coordinated with one P atom from **L** and one or two pyridine N atoms from different **L**. All the Ag–P bond lengths are close to 2.4 Å, while Ag–N distances are in the range of 2.178–2.507 Å. Two pyridine rings, shown as uncoordinated in Fig. 2, have Ag–N distances too large (about 2.7 Å) to be bonded. The interatomic distances between two Ag–Ag pairs (2.90–2.92 Å) are significantly shorter than the sum of their VdW radii (3.44 Å),[67] indicating metallophilic interactions.

The cationic part of **5** is formed by three Ag(I) ions P,P′-bridged by three **L** ligands to form a 15-membered metalocycle with P–Ag–P angles of 166.9° and 164.9° (Fig. 2). The six remaining Ag(I) ions are located at the periphery of the metalocycle and each are N,N′-chelated by the CH_2Py arms of two neighboring **L** ligands. This results in six short contacts between the "peripheral" and "central" Ag(I) ions of 2.99–3.03 Å (>88% $\sum r_{vdW(Ag-Ag)}$),[67] suggesting argentophilic interactions. In addition, the two "peripheral" Ag^+ ions are weakly associated with two NO_3^- ions in a bidentate chelating manner (d_{Ag-O} ≈ 2.69 ± 0.03 Å). At the center of the 15-membered metallocycle of **5**, a disordered NO_3^- anion is also captured *via* Ag–O contacts of 2.674–2.694 Å.

The packing of **6** consists of two independent $[Au_2Ag_4L_2(NO_3)_2(H_2O)]^{4+}$ cations charge-balanced by eight NO_3^- anions. In the cations, two Au(I) ions are P,P′-bridged by two **L** ligands, and the four Ag(I) ions are chelated by four pairs of CH_2Py arms, affording two bent Ag–Au–Ag cluster units (∠Ag–Au–Ag = 125.4–145.3°). While the intramolecular Au–Au distance of ~3.9 Å clearly rules out metallophilic interactions, the four Au–Ag distances of 2.96–3.05 Å (<90% $\sum r_{vdW(Au-Ag)}$)[67] indicate such interactions. Note that the adjacent Ag(I) ions of the $AuAg_2$ units of **6** are bridged by two NO_3^- ions (d_{Ag-O} ≈ 2.78–2.85 Å), and one Ag atom is also ligated by an H_2O ligand (d_{Ag-O} ≈ 2.62 Å).

The structure of the $[Au_2Cu_4L_2(\mu_2\text{-}Cl)_2]^{4+}$ cation of **7** is comparable to that of the cation of **6**. The two Au(I) atoms of **7** are P,P′-bridged by two **L** ligands, and the four Cu(I) ions are che-

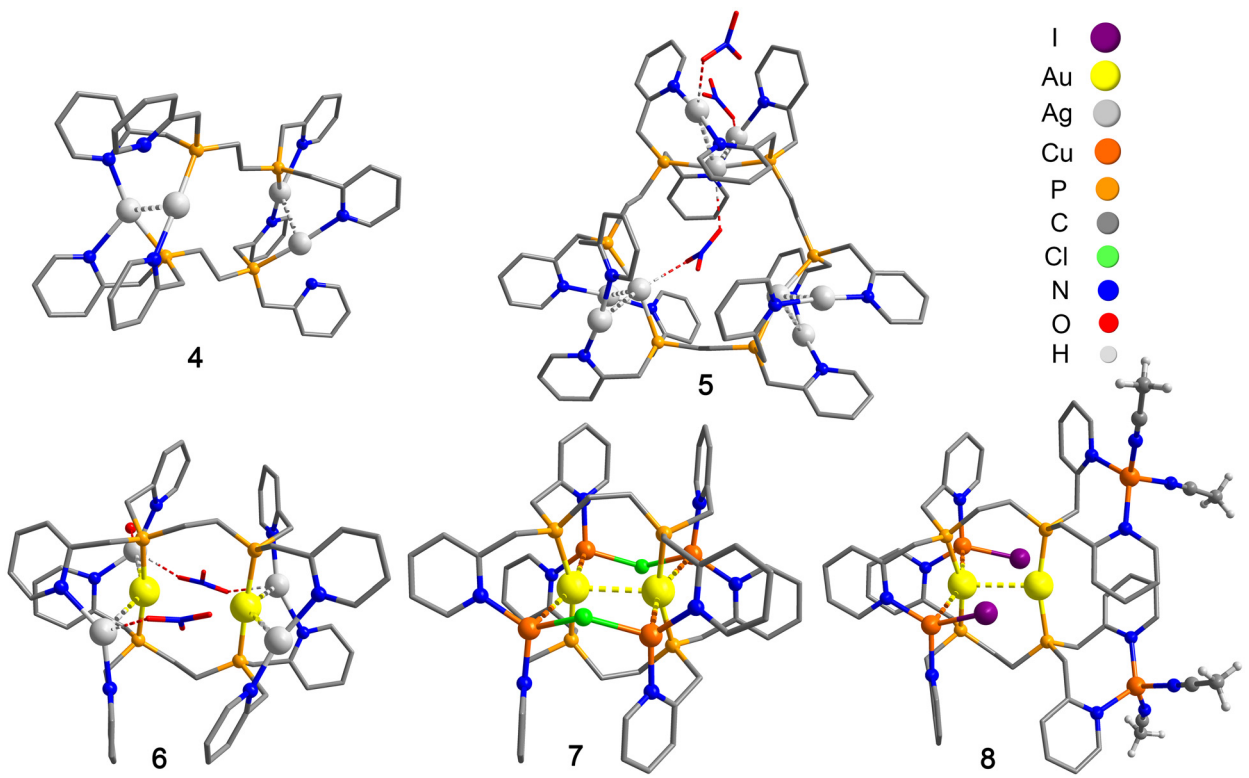

Fig. 2 X-Ray derived structures of **4–8**. The aromatic H-atoms, counterions and solvate molecules are omitted for clarity.

lated by four pairs of CH_2Py arms. Moreover, each copper atom is coordinated by a μ_2-Cl atom (∠Cu–Cl–Cu = 128.66°). The formed Au_2Cu_4 cluster core adopts a distorted H-shaped geometry (∠Cu–Au–Cu = 157.4°) with one Au–Au and four Cu–Au metallophilic contacts of 3.064 Å (92% $\sum r_{vdW(Au-Au)}$) and ~2.81 Å (92% $\sum r_{vdW(Au-Cu)}$), respectively.

In the $[Au_2Cu_4I_2L_2(MeCN)_4]^{4+}$ cation of **8**, each Au(I) ion is coordinated by two phosphorus atoms from different **L** ligands (∠P–Au–P = 161.29 and 161.94°) to form an Au–Au contact of 3.115 Å (94% $\sum r_{vdW(Au-Au)}$). The two Cu(I) atoms form short contacts with the same Au(I) center (2.78–2.82 Å, <92% $\sum r_{vdW(Au-Cu)}$), and each of them is coordinated by two pyridine N atoms of different **L** ligands as well as by one I atom. Each of the two remaining Cu(I) ions is N,N′-chelated by the CH_2Py arms of the same **L** ligands, and MeCN auxiliary ligands (d_{Cu-N} = 2.05 Å) complete a tetrahedral Cu@N_4 geometry (τ_4 = 0.84–0.88).

Thus, the flexibility of the ligand **L**, which is determined by the presence of $P(CH_2)_2P$ and $PyCH_2P$ fragments, allows for the stabilization of diverse cluster units. The intraligand P–P distance in **L** can range from 3.69 Å to 4.49 Å, and the P–N distance in the $PyCH_2$ arms varies from 2.83 to 3.56 Å. Again, the flexibility of the $P(CH_2)_2P$ and $PyCH_2P$ moieties also allows for a wide variability in the angles between the lone pairs on the N and P donor sites. As a results, the $P(CH_2)_2P$ of **L** unit can stabilize both well-separated M(I) ions (as in **3a** and **3b**) and two closely spaced M(I) ions (as in **1**, **2** and **4–8**). In turn, the PCH_2Py unit of **L** exhibits both P,N-bridging and P,N-chelating modes. In contrast, more "rigid" ligands (Scheme 1) do not exhibit P,N-chelating mode due to the shorter and less variable P–N distance in the PyP unit.

The compounds obtained were characterized by NMR and mid-IR spectroscopy, and their compositions were confirmed by microanalysis data. The powder X-ray diffraction analysis data also confirm the phase purity of the synthesized bathes (Fig. S10†). In ^{1}H NMR spectra of **1–5** and **7**, the protons of the CH_2Py and $P(CH_2)_2P$ moieties resonate in their typical regions (Fig. S11–16†). In the $^{31}P\{^1H\}$ NMR spectra of **1–5** and **7**, the ligand's phosphorus atoms appear as singlets at 33.2, 24.8, 36.5, −6.5, −3.54 and 29.3, and ppm, respectively, and PF_6^- anions of **1**, **4**, **7** and **8** is presented as a typical septet (J_{P-F} ≈ 712 Hz) (Fig. S17–21 and S23†). The ^{1}H NMR spectra of **6** and **8** show a set of very broad resonances that are difficult to assign to specific protons. Such a scenario is probably caused by a slow exchange equilibrium between dissociated species that is typical behavior for Au^I–Ag^I and Au^I–Cu^I complexes.[29] This assumption is also indirectly confirmed by the presence of two ^{31}P resonances in solutions of **6** and **8** (Fig. S22 and S24†).

The mid-IR spectra of **1–8** (Fig. S25†) are consistent with the structural data and show specific vibrations from the supporting ligands and counter-ions. For instance, the C≡C bonds of **3a** appears as a $\nu_{C\equiv C}$ stretching band at 2112 cm^{-1}, and the MeCN ligands in **8** appear as a weak $\nu_{C\equiv N}$ band at 2253–2270 cm^{-1}. The thermogravimetric analysis confirms the presence of the solvate molecules in **3a**·EtOH, **5**·8H_2O, **6**·2H_2O and **7**·2Me_2CO, and MeCN ligands in **8**, showing the corresponding steps in the range of 75–175 °C (Fig. S26†).

Electronic structure and absorption spectra

To investigate the electronic structure of **1–8**, DFT calculations were performed on the molecules of **2** and **3a** as well as on the $[Au_2L_2]^{2+}$ (**1**), $[Ag_4L_2]^{4+}$ (**4**), $[Ag_9L_3(NO_3)]^{8+}$ (**5**), $[Au_2Ag_4L_2(NO_3)_2(H_2O)]^{4+}$ (**6**), $[Au_2Cu_4L_2(\mu_2\text{-}Cl)_2]^{4+}$ (**7**) and $[Au_2Cu_4L_2I_2(MeCN)_4]^{4+}$ (**8**) species (for details see §8, ESI†). The highest occupied and lowest unoccupied molecular orbitals (HOMO and LUMO) are shown in Fig. 3, while HOMO−1 to LUMO+1 plots are displayed in Fig. S27–34.† The HOMO of **1** includes only the metal s- and d-orbitals, while the HOMOs of the other complexes are also contributed by halide's lone pairs (**2**, **7** and **8**), or the p-orbitals from the **L** ligands (**4**, **5**), C≡C (**3a**) or NO_3^- (**6**) groups. The LUMOs of **2–4**, **6** and **8** are purely pyridine π-orbitals, whereas LUMOs of **1**, **5** and **7** consist mainly p_σ orbitals from Au–Au or Ag–Ag units, and, in the case of **1** and **5**, are also admixed with pyridine π-orbitals.

To understand the electronic transitions leading to the excited states of **1–8**, electronic absorption spectra (EAS) were analyzed (Fig. 4). The EAS profiles of **1–8** show a strong absorption band at around 260 nm ($\varepsilon \approx 25\,000$–$56\,000$ M^{-1} cm^{-1}). In the case of **3a**, this band has a vibronically resolved structure ($\tilde{\nu}$ = 1590 cm^{-1}), likely caused by π → π* transitions in the {C≡C-Ph} moiety. In the 280–400 nm region, less intense absorptions (ε < 15 000 M^{-1} cm^{-1}) appear for all compounds studied. The TD-DFT calculated absorption patterns reasonably match the experimental EAS profiles of **1–8** (Fig. S35†), indicating that the low-energy region is conditioned by the CT transitions. In particular, the following types of the CT transitions are specific: (Au + L)AuLCT (**1**), (Au + I)LCT (**2**), (Au + C≡C)LCT (**3a**), (Ag + L)LCT (**4**), (Ag + NO_3^-)LXCT (**5**), (Au + Cu + X)LXCT (X = NO_3^-, **6**), (Cu + Cl)AuCT (**7**), (Au + Cu + I + MeCN)LCT (**8**). For clarity, these assignments are also outlined in the Table 1. Therefore, only in complex **7**, ligand **L** orbitals do not participate in low-energy transitions. In all other cases, the pyridine π-orbitals of **L** participate in the lowest charge-transfer transitions. Natural transition orbital (NTO) analysis corroborates the above assignments by showing that the "electron" and "hole" orbitals for the $S_0 \rightarrow S_1$ or $S_0 \rightarrow S_2$ transitions (Tables S3–S11†) closely resemble the virtual and occupied molecular orbital pairs from ground-state calculations. Again, in the lowest singlet–singlet transitions, the "electron" NTOs of **1–6** and **8** are primarily delocalized over the π-orbitals of the L moieties. The NTOs' "holes" are largely contributed by the metal(I) atoms, alongside halides and other ancillary ligands. In the case of **1** and **4**, NTOs' "holes" are also admixed by π-orbitals of the L moieties.

Regarding the effect of metallophilic interactions, note that the LUMO of **7** exhibits Au–Au antibonding character and is involved in the lowest singlet–singlet transition. NTO analysis shows that the "electron" NTOs of the lowest $S_0 \rightarrow S_1$ and $S_0 \rightarrow T_1$ transitions are localized on the Au p-orbitals. Thus, the emission of complex **7** has been assigned to the (Cu + I)AuCT type. For all other complexes, metal-centered antibonding NTO

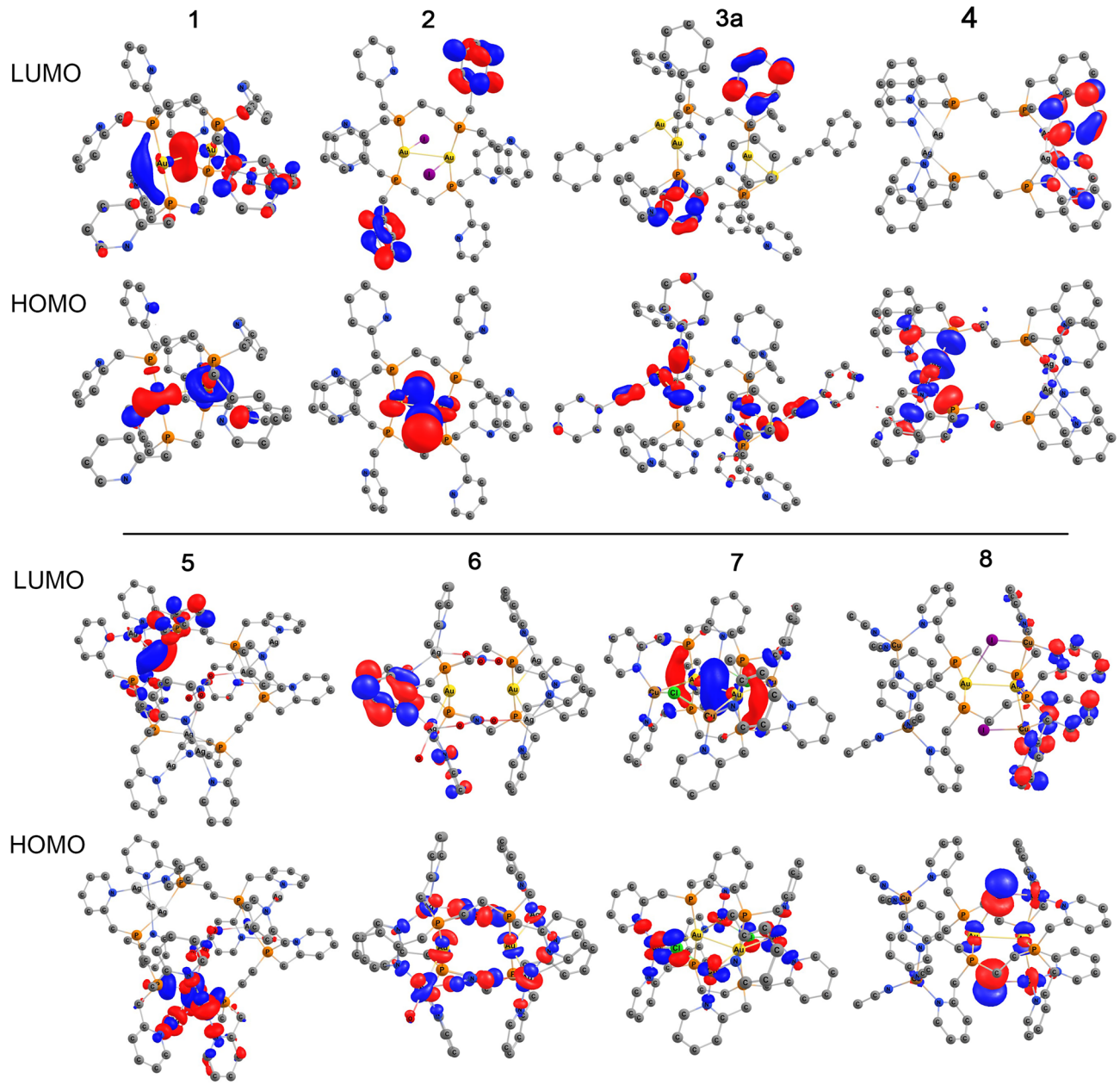

Fig. 3 Ground state frontier orbitals for **2** and **3a** molecules as well as cations of **1** and **4–8**. The H atoms are omitted for clarity.

orbitals do not contribute to the lowest $S_0 \rightarrow S_1$ and $S_0 \rightarrow T_1$ transitions.

Photophysical properties

At ambient temperature, polycrystalline samples of **2–4** and **6–8** demonstrate moderate to strong photoluminescence (PL) in the green to orange region (Fig. 5a), whereas compounds **1** and **5** are non-emissive. The emission and excitation spectra of **2–4** and **6–8** are plotted in Fig. 5b, c, and the corresponding parameters are listed in Table 1. The PL profiles of **2**, **4** and **6–8** are represented by single bands, whose maxima vary from 505 to 635 nm, and half-peak widths are in the order of 3189–3780 cm^{-1}. In the excitation spectra (Fig. 5b), broad featureless bands appear falling between 455 nm (for **6**) and 570 nm (**4**). No excitation-dependent behaviour was observed for these emitters (Fig. S36†). The large Stokes shifts (4652–6514 cm^{-1}) and the microsecond PL times indicate that **2–4** and **6–8** manifest phosphorescence at 298 K, which is typical for the related clusters. Taking into account the literature data and the results of our TD DFT NTO calculations (see above), the observed PL can be tentatively assigned to (Au + L)AuLCT (**1**), (Au + I)LCT (**2**), (Au + C≡C)LCT (**3a**), (Ag + L)LCT (**4**), (Ag + NO_3^-)LXCT (**5**), (Au + Cu + X)LXCT (X = NO_3^-, **6**), (Cu + Cl)AuCT (**7**), and (Au + Cu + I + MeCN)LCT (**8**) types, respectively. It should be noted, however, that the TADF mechanism can't be completely excluded for Cu(I)–Au(I) clusters **7** and **8**,

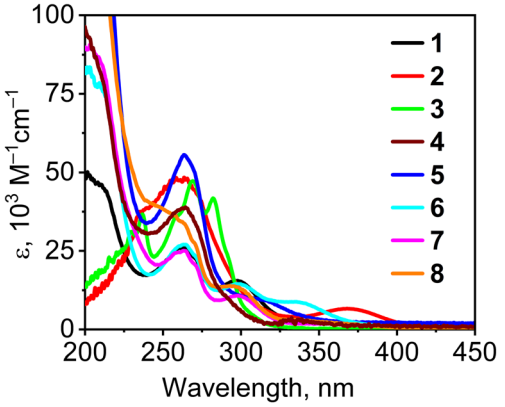

Fig. 4 EAS profiles recorded for solutions in MeCN (**1**, **4**, **6–8**), CH_2Cl_2 (**2**, **3**) and H_2O (**5**).

which show an abnormal temperature-dependent PL behavior (see below). The measured PLQYs vary from low (1–4% for **3a, b**, **4**) to high (77% for **2**), and are moderate (15–40%) for **6–8**. The PLQY of **2** is among the highest values for AuI-based phosphine complexes.[71–73]

A special case are Au(I)-alkynyl complexes **3a** and **3b** which exhibit multiband PL typical of the related complexes.[68,74] The emission profiles of both complexes are very similar in the 400–540 nm range, where a high-energy (HE) band (λ_{max} = 515 nm) with a vibronically resolved shoulder at 420–465 nm is observed (Fig. 5c and S44†). Polymer **3b**, regardless of the excitation wavelength, shows a prominent low-energy (LE) band at 630 nm (Fig. S44†). In the case of **3a**, a similar LE band (λ_{max} = 580 nm) is almost imperceptible at 300–400 nm excitation, but appears clearly at ≥440 nm excitation (Fig. S44†). Both the HE and LE bands of **3a,b** have decay times in the microsecond range (Table 1). Based on the previous works and our DFT calculation results, the HE bands can be assigned to the $\pi^*_{Py} \rightarrow (d_{Au} + \pi_{C\equiv C})$ transitions.[68,74–77] The LE band likely belongs to the $(d_{\delta^*})^1(p_\sigma)^1$ triplet state, which originates from the Au–Au interactions taking place in both dimer **3a** and polymer **3b**. The vibronic structure observed for the HE bands of **3a,b** is likely conditioned by $\nu_{C\equiv C}$ vibrations of the alkynyl groups.

Cooling to 77 K brings about only a slight PL enhancement for **2–4** and **6**, while **7** and **8** show a pronounced thermochromic PL (see CIE diagrams in Fig. 5d and e). The measured temperature-dependent PL spectra of **7** and **8** (Fig. 5d and e) agree with the visually observed changes in the PL color and intensity. Both **7** and **8** show a pronounced bathochromic shift of λ_{max} by 556 and 965 cm^{-1}, respectively, however, their integrated PL intensities change differently with temperature (Fig. 5f). When **7** is cooled from 298 to 120 K, its PL intensity gradually decreases, and when further cooling to 77 K, it becomes slightly larger than at 298 K. In contrast, the PL intensity of **8** abnormally decreases by 25% when passing from 298 K to 77 K, thus showing a negative thermal quenching (NTQ) behavior. It should be noted that NTQ emitters are very rare among coordination compounds,[78–80] and NTQ-active Au(I) complexes are so far unknown, not to mention Au(I)–Cu(I) clusters. To our surprise, the temperature dependences of the PL lifetimes [$\tau(T)$ plots, Fig. 5g] adopt a TADF-specific shape, and they are well fitted by the equation for the TADF model[81] (see p. S50 in ESI† for details). The fitting-derived singlet–triplet energy gaps of 518 and 506 cm^{-1} (for **7** and **8**, respectively) are sufficiently small (<1200 cm^{-1}) for TADF realization at ambient temperature, and they are comparable with those for Cu(I) complexes.[81,82] The abnormal NTQ behavior for **8** can be reasonably explained the basis of TADF mechanism. The $\tau(T)$ curves (Fig. 5g) indicate that the S_1 state is emissive at 298 K (TADF regime), whereas at 77 K, when TADF is largely frozen out, the T_1 state is active (phosphorescence regime). The NTQ behaviour of **8** can be explained by assuming that the ratio of the non-radiative decay rate to the radiative one (k_{nr}/k_r) for the T_1 state is higher than that for the S_1 state (see Fig. S46† and discussion below). In turn, the near-zero PL thermal quenching of **7** is due to a close k_{nr}/k_r ratio for its T_1 and S_1 states.

In contrast to the other clusters, **2** and **6** exhibited yellow and green PL in solution with PLQYs of 5% and 6%, respectively (Fig. S47†). The PL profile of CH_2Cl_2 solution of **2** shows one band at λ_{max} = 540 nm (τ_1 = 16 ns, τ_2 = 64 ns), while the aqueous solution of **6** shows two PL bands at λ_{max} = 510 nm (τ_1 = 219 ns, τ_2 = 63 ns) and 625 nm (τ = 0.26 μs). Since the ^{31}P NMR data point to a dissociation of **6** in solution, it remains unclear whether the two emission bands are belonged to **6** or

Table 1 The absorption characteristics of **1–8** in solutions and solid-state PL properties of **2–4** and **6–8** at 298 K

Compound	λ_{abs}, nm ($\varepsilon \times 10^3$ M^{-1} cm^{-1})	Character of the low-energy absorption	λ_{em}, nm	PL time, μs	PLQY, %
1	206 (47), 263 (27), 298 (16)	(Au + L)AuLCT	—	—	—
2 [a]	238^{sh} (38), 261 (49), 370 (7)	(Au + I)LCT	550	2.7	77
3a [b]	229 (31), 237 (37), 258^{sh} (37), 268 (47), 283 (42)	(Au + C≡C)LCT	515	33	1
3b [a]			515 (HE), 610 (LE)	78 (HE), 445 (LE)	1
4 [c]	205^{sh} (89), 264 (34), 335 (3)	(Ag + L)LCT	635	4.3	4
5	205 (167), 263 (58), 318^{sh} (10)	(Ag + NO_3^-)LXCT	—	—	—
6 [c]	200 (84), 263 (27), 298 (14), 335 (9)	(Au + Cu + X)LXCT (X = NO_3^-)	505	13	15
7 [d]	198 (90), 263 (25), 299 (11)	(Cu + Cl)AuCT	618	5.4	40
8 [e]	204 (132), 252^{sh} (38), 295 (14)	(Au + Cu + I + MeCN)LCT	585	4.0	38

[a] λ_{ex} = 350 nm. [b] λ_{ex} = 300 nm. [c] λ_{ex} = 380 nm. [d] λ_{ex} = 460 nm. [e] λ_{ex} = 420 nm.

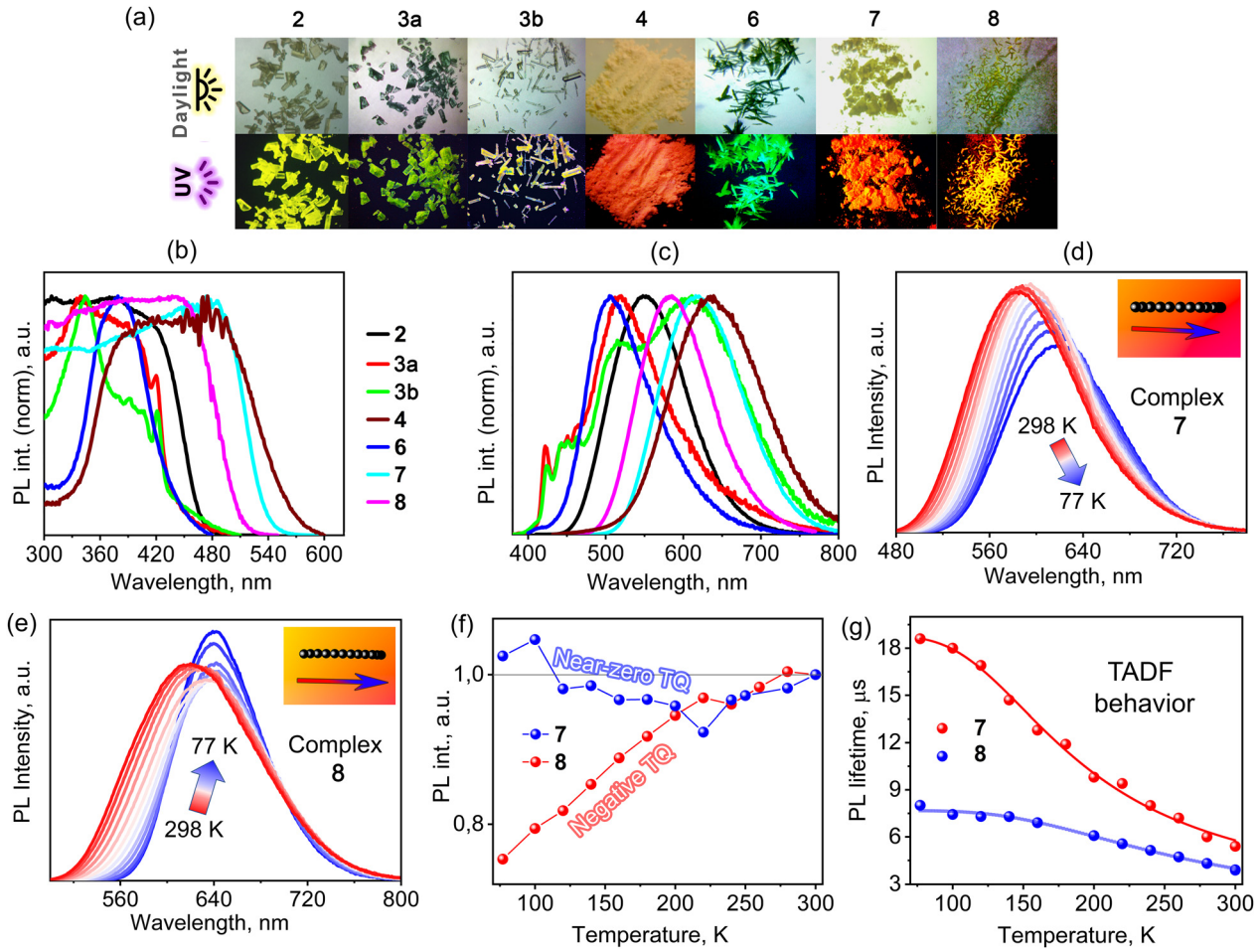

Fig. 5 (a) Microphotography of samples of **2**–**4** and **6**–**8** under daylight and UV-light; (b) solid state excitation spectra at 298 K (the excitation profile of **3a**,**b** correspond to their HE emission band); (c) solid state PL spectra (λ_{ex} = 360 nm); (d) temperature-dependent PL spectra of **7** at λ_{ex} = 440 nm (insert: changing in PL color in CIE coordinates); (e) temperature-dependent PL spectra of **8** at λ_{ex} = 420 nm (insert: changing in PL color in CIE coordinates); (f) integrated PL intensities of **7** and **8** *versus* temperature; (g) PL lifetimes of **7** and **8** *versus* temperature. The fitting curves are derived from the TADF model equation.[81]

to its dissociation products. The slight increase in PL during deaeration of solutions **2** and **6** indicates the manifestation of phosphorescence.

Application of 2 and 6 as vapor-responsive anticounterfeiting inks

Luminescent coinage metal complexes are currently attracting much attention as stimuli-responsive materials,[83–87] and anticounterfeiting dyes. In this regard, the coinage metal(I) complexes have been poorly studied, and to our knowledge, coinage metal clusters are still unexplored for anticounterfeiting. Serendipitously, we discovered that the photoluminescence (PL) of **2** deposited on paper was reversibly quenched upon exposure to acetone, whereas vapors of other tested solvents (including H_2O, MeOH, Et_2O, hexane, EtOH, i-PrOH, EtOAc, THF, DMF, 1,4-dioxane, C_6H_6, C_6H_5Br, C_6F_6, CCl_4) had no significant effect on the PL. Notably, the PL of other highly emissive clusters (**6**–**8**) remained stable under all tested solvent vapors. Inspired by this interesting finding, we used these clusters as innovative anticounterfeiting dyes. Diluted solutions of **2** and **6** were spotted onto filter paper. The resulting labels are completely invisible in daylight, but are clearly visible under UV light as green (from **2**) and cyan (from **6**) spots (Fig. 6a). When the paper is immersed in a beaker with acetone vapors, the green spots disappear immediately, while the cyan spots remain unchanged. When the paper is removed from the beaker, the green spots immediately reappear. As shown in supplemented video file, such "encryption–decryption" process is very fast and repeatable. Furthermore, the PL intensity of **2** was investigated over a range of acetone concentrations (0–3132 ppm). As shown in Fig. 6c, the PL emission intensity of the paper test strip decreases with increasing acetone molar concentration (C_a). A Stern–Volmer (SV) plot of I_0/I (where I_0 and I represent the initial and current PL intensities, respectively) *versus* C_a demonstrates characteristic quenching behavior (Fig. 6c, insert), fitting the equation: $I_0/I = 1.40 \times 10^{-3}[C_a] + 0.88$ ($K_{SV} = 1.40 \times 10^{-3}$ ppm^{-1}). Notably, the SV plot exhibits excellent line-

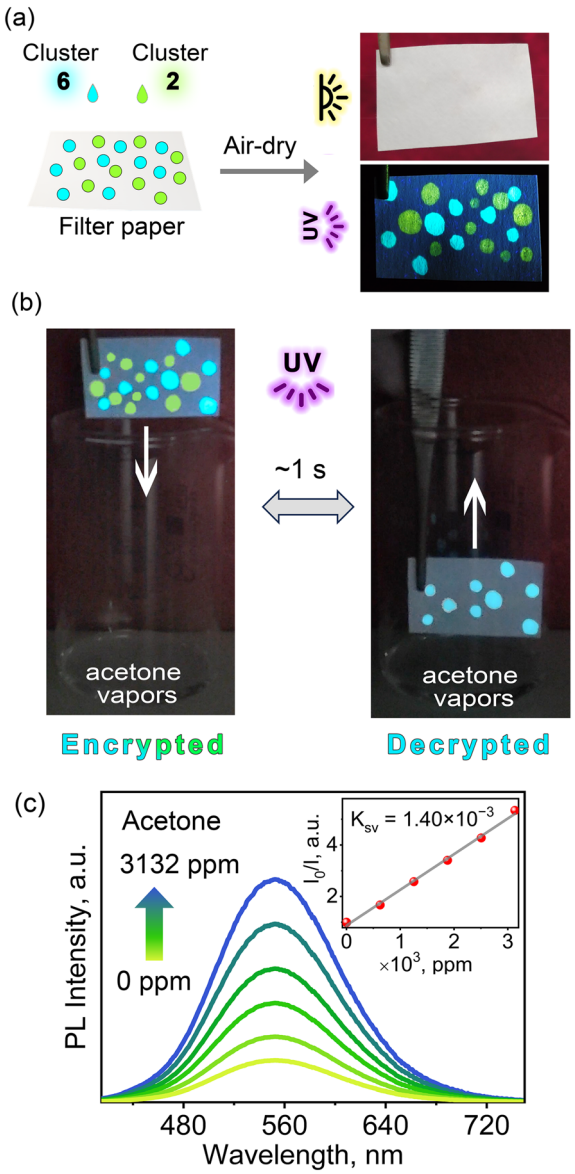

Fig. 6 Anticounterfeiting application of **2** and **6**: (a) fabrication of labels; (b) rapid and reversible quenching of green luminescence of **2** in acetone vapours (25 °C, 365 nm light), see also ESI video file;† (c) PL spectra of a **2**-impregated test strips under different concentrations of acetone (298 K, λ_{ex} = 400 nm). Insert: Stern–Volmer plot.

arity (R^2 = 0.997) across the entire concentration range. These preliminary results suggest that cluster **2** shows potential for on-site acetone detection when coupled with a portable spectrometer. Although an explanation of this effect is beyond the scope of this work, by analogy with work[83] it can be proposed that acetone quenches the T_1 state of **2** *via* a photo-induced electron transfer mechanism.

Conclusions

In summary, bis[bis(pyridin-2-ylmethyl)phosphino]ethane – an innovative multidentate ligand – has been introduced into the chemistry of group 11 metal clusters. The flexibility of the CH_2Py arms allows this ligand to stabilize new cluster units *via* P,P′(N,N′)$_2$-bridging coordination, which is not possible for "rigid" diphosphines with direct phosphorus-pyridine linkage. On the other hand, the symmetric structure of our ligand predetermines the (pseudo)symmetric geometry of the clusters thereof. By exploiting the features of the above ligand, we have synthesized homo- and heterometallic clusters characterized by unprecedented structures and the presence of multiple metallophilic Au–X (X = Cu, Ag, Au) or Ag–Ag contacts. Most of the designed clusters exhibited a weak to very strong solid-state photoluminescence at ambient temperature, which is attributed to the metal-involved charge transfer excited states. Surprisingly, the $[Au_2Cu_4L_2I_2(MeCN)_4]^{4+}$ cluster increases its PL intensity upon warming from 77 to 298 K, revealing an abnormal (negative) thermal quenching behavior. Moreover, the $[Au_2L_2I_2]$ cluster has been highlighted as an original anti-counterfeiting dye using vapor stimuli for (de)coding.

Fundamentally, these results highlight the diphosphine ligands with flexible CH_2Py arms as a new efficient platform for the design of unprecedented cluster ensembles. From a practical perspective, some of the synthesized compounds can be considered as emitters for OLED application and emissive for advanced data security.

Conflicts of interest

There are no conflicts to declare.

Data availability

The data supporting this article have been included as part of the ESI.†

Acknowledgements

This work was supported by Russian Science Foundation (project 19-73-20196-p) and the Ministry of Science and Higher Education of the Russian Federation. I. Yu. B. thanks the Multi-Access Chemical Research Center SB RAS for single crystal X-ray diffraction measurements.

References

1 I. Chakraborty and T. Pradeep, Atomically precise clusters of noble metals: emerging link between atoms and nanoparticles, *Chem. Rev.*, 2017, **117**, 8208–8271.
2 R. S. Dhayal, W. E. van Zyl and C. W. Liu, Polyhydrido copper clusters: synthetic advances, structural diversity, and nanocluster-to-nanoparticle conversion, *Acc. Chem. Res.*, 2016, **49**, 86–95.
3 S. K. Emashova, A. A. Titov, A. F. Smol'yakov, A. Y. Chernyadyev, I. A. Godovikov, M. I. Godovikova,

P. V. Dorovatovskii, A. A. Korlykov, O. A. Filippov and E. S. Shubina, Emissive silver(I) cyclic trinuclear complexes with aromatic amine donor pyrazolate derivatives: way to efficiency, *Inorg. Chem. Front.*, 2022, **9**, 5624–5634.

4 A. Laguna, T. Lasanta, J. M. López-de-Luzuriaga, M. Monge, P. Naumov and M. E. Olmos, Combining aurophilic interactions and halogen bonding to control the luminescence from bimetallic gold–silver clusters, *J. Am. Chem. Soc.*, 2010, **132**, 456–457.

5 T.-H. Chiu, J.-H. Liao, R. P. B. Silalahi, M. N. Pillay and C. W. Liu, Hydride-doped coinage metal superatoms and their catalytic applications, *Nanoscale Horiz.*, 2024, **9**, 675–692.

6 A. V. Chupina, V. V. Yanshole, V. S. Sulyaeva, V. V. Kokovkin, P. A. Abramov and M. N. Sokolov, Self-assembly patterns of non-metalloid silver thiolates: structural, HR-ESI-MS and stability studies, *Dalton Trans.*, 2022, **51**, 705–714.

7 V. V. Volchek, A. S. Berezin, M. N. Sokolov and P. A. Abramov, Stabilization of $\{Ag_{20}(StBu)_{10}\}$ and $\{Ag_{19}(StBu)_{10}\}$ toroidal complexes in DMSO: HPLC-ICP-AES, PL, and structural studies, *Inorganics*, 2022, **10**, 225.

8 H. Schmidbaur and A. Schier, Aurophilic interactions as a subject of current research: an up-date, *Chem. Soc. Rev.*, 2012, **41**, 370–412.

9 H. Schmidbaur and A. Schier, Argentophilic Interactions, *Angew. Chem., Int. Ed.*, 2015, **54**, 546–784.

10 S. Sculfort and P. Braunstein, Intramolecular d^{10} – d^{10} interactions in heterometallic clusters of the transition metals, *Coord. Chem. Rev.*, 2011, **40**, 2741–2760.

11 V. Vreshch, W. Shen, B. Nohra, S.-K. Yip, V. W.-W. Yam, C. Lescop and R. Réau, Aurophilicity versus mercurophilicity: impact of d^{10}–d^{10} metallophilic interactions on the structure of metal-rich supramolecular assemblies, *Chem. – Eur. J.*, 2012, **18**, 466–477.

12 M. E. S. Moussa, S. Evariste, H. Wong, L. Le Bras, C. Roiland, L. Le Polles, B. Le Guennic, K. Costuas, V. W. Yam and C. Lescop, A solid state highly emissive Cu(I) metallacycle: promotion of cuprophilic interactions at the excited states, *Chem. Commun.*, 2016, **52**, 11370–11373.

13 K. F. Baranova, A. A. Titov, J. R. Shakirova, V. A. Baigildin, A. F. Smol'yakov, D. A. Valyaev, G.-H. Ning, O. A. Filippov, S. P. Tunik and E. S. Shubina, Substituents' effect on the photophysics of trinuclear copper(I) and silver(I) pyrazolate–phosphine cages, *Inorg. Chem.*, 2024, **63**, 16610–16621.

14 H. Yu, B. Rao, W. Jiang, S. Yang and M. Zhu, The photoluminescent metal nanoclusters with atomic precision, *Coord. Chem. Rev.*, 2019, **378**, 595–617.

15 X. Zhang and H. Xu, Electroluminescent clusters, *Angew. Chem., Int. Ed.*, 2024, **63**, e202317597.

16 V. W.-W. Yam, V. K.-M. Au and S. Y. Leung, Light-emitting self-assembled materials based on d^8 and d^{10} transition metal complexes, *Chem. Rev.*, 2015, **115**, 7589–7728.

17 J. Ma, J. Schaab, S. Paul, S. R. Forrest, P. I. Djurovich and M. E. Thompson, Luminescent bimetallic two-coordinate gold(I) complexes utilizing Janus carbenes, *J. Am. Chem. Soc.*, 2023, **145**, 20097–20108.

18 K. Han and Z. Xia, Coinage metal cluster scintillator for X-ray imaging, *ACS Cent. Sci.*, 2023, **9**, 1263–1265.

19 N. Zhang, L. Qu, S. Dai, G. Xie, C. Han, J. Zhang, R. Huo, H. Hu, Q. Chen, W. Huang and H. Xu, Intramolecular charge transfer enables highly-efficient X-ray luminescence in cluster scintillators, *Nat. Commun.*, 2023, **14**, 2901.

20 X. He and V. W.-W. Yam, Luminescent gold(I) complexes for chemosensing, *Coord. Chem. Rev.*, 2011, **255**, 2111–2123.

21 E. S. Smirnova, J. M. M. Molina, A. Johnson, N. A. G. Bandeira, C. Bo and A. M. Echavarren, Polynuclear gold $[AuI]_4$, $[AuI]_8$, and bimetallic $[AuI_4AgI]$ complexes: C–H functionalization of carbonyl compounds and homogeneous carbonylation of amines, *Angew. Chem., Int. Ed.*, 2016, **55**, 7487–7491.

22 Z.-M. Xiao, J.-X. Yang, X. Chen, W.-J. Tang, S.-K. Peng, D.-B. Hao, Z.-P. Zhao, J. Zheng and D. Li, A fluorescence–phosphorescence dual-emissive $Cu_3(pyrazolate)_3$ complex with highly tunable emission colours for anticounterfeiting and temperature sensing, *Inorg. Chem. Front.*, 2024, **11**, 1808–1818.

23 S. Perruchas, Molecular copper iodide clusters: a distinguishing family of mechanochromic luminescent compounds, *Dalton Trans.*, 2021, **50**, 12031–12044.

24 A. Kobayashi and M. Kato, Stimuli-responsive luminescent copper(I) complexes for intelligent emissive devices, *Chem. Lett.*, 2017, **46**, 154–162.

25 Q. Benito, B. Baptiste, A. Polian, L. Delbes, L. Martinelli, T. Gacoin, J.-P. Boilot and S. Perruchas, Pressure control of cuprophilic interactions in a luminescent mechanochromic copper cluster, *Inorg. Chem.*, 2015, **54**, 9821–9825.

26 H. Ito, T. Saito, N. Oshima, N. Kitamura, S. Ishizaka, Y. Hinatsu, M. Wakeshima, M. Kato, K. Tsuge and M. Sawamura, Reversible mechanochromic luminescence of $[(C_6F_5Au)_2(\mu\text{-}1,4\text{-diisocyanobenzene})]$, *J. Am. Chem. Soc.*, 2008, **130**, 10044–10045.

27 R. P. B. Silalahi, T.-H. Chiu, J.-H. Kao, C.-Y. Wu, C.-W. Yin, Y.-C. Liu, Y. J. Chen, J.-Y. Saillard, M.-H. Chiang and C. W. Liu, Synthesis and luminescence properties of two-electron bimetallic Cu–Ag and Cu–Au nanoclusters via copper hydride precursors, *Inorg. Chem.*, 2021, **60**, 10799–10807.

28 I. S. Krytchankou, D. V. Krupenya, A. J. Karttunen, S. P. Tunik, T. A. Pakkanen, P.-T. Chou and I. O. Koshevoy, Triphosphine-supported bimetallic AuI–MI (M = Ag, Cu) alkynyl clusters, *Dalton Trans.*, 2014, **43**, 3383–3394.

29 M. T. Dau, J. R. Shakirova, A. J. Karttunen, E. V. Grachova, S. P. Tunik, A. S. Melnikov, T. A. Pakkanen and I. O. Koshevoy, Coinage metal complexes supported by the tri- and tetraphosphine ligands, *Inorg. Chem.*, 2014, **53**, 4705–4715.

30 S.-K. Peng, Z. Lu, M. Xie, Y.-L. Huang, D. Luo, J.-N. Wang, X.-W. Zhu, X. Li, X.-P. Zhou and D. Li, Unexpected structural transformation into noria-like Ag_{13} metal clusters and

a copper-doping induced boost in photoluminescence, *Chem. Commun.*, 2020, **56**, 4789–4792.

31 J. C. F. Colis, C. Larochelle, E. J. Fernández, J. M. López-de-Luzuriaga, M. Monge, A. Laguna, C. Tripp and H. Patterson, Tunable photoluminescence of closed-shell heterobimetallic Au–Ag dicyanide layered systems, *J. Phys. Chem. B*, 2005, **109**, 4317–4323.

32 M. K. Rong, F. Holtrop, J. C. Slootweg and K. Lammertsma, Enlightening developments in 1,3-P,N-ligand-stabilized multinuclear complexes: A shift from catalysis to photoluminescence, *Coord. Chem. Rev.*, 2019, **382**, 57–68.

33 I. D. Strelnik, I. R. Dayanova, I. E. Kolesnikov, R. R. Fayzullin, I. A. Litvinov, A. I. Samigullina, T. P. Gerasimova, S. A. Katsyuba, E. I. Musina and A. A. Karasik, The assembly of unique hexanuclear copper(I) complexes with effective white luminescence, *Inorg. Chem.*, 2019, **58**, 1048–1057.

34 K. Chen and V. J. Catalano, Luminescent thermochromism in a gold(I)–copper(I) phosphine–pyridine complex, *Eur. J. Inorg. Chem.*, 2015, 5254–5261.

35 D. Volz, Y. Chen, M. Wallesch, R. Liu, C. Fléchon, D. M. Zink, J. Friedrichs, H. Flügge, R. Steininger, J. Göttlicher, C. Heske, L. Weinhardt, S. Bräse, F. So and T. Baumann, Bridging the efficiency gap: fully bridged dinuclear Cu(I)-complexes for singlet harvesting in high-efficiency OLEDs, *Adv. Mater.*, 2015, **27**, 2538–2543.

36 A. V. Artem'ev, M. Z. Shafikov, A. Schinabeck, O. V. Antonova, A. S. Berezin, I. Y. Bagryanskaya, P. E. Plusnin and H. Yersin, Sky-blue thermally activated delayed fluorescence (TADF) based on Ag(I) complexes: strong solvation-induced emission enhancement, *Inorg. Chem. Front.*, 2019, **6**, 3168–3176.

37 A. Y. Baranov, M. I. Rakhmanova, X. Hei, D. G. Samsonenko, D. V. Stass, I. Y. Bagryanskaya, M. R. Ryzhikov, V. P. Fedin, J. Li and A. V. Artem'ev, A new subclass of copper(I) hybrid emitters showing TADF with near-unity quantum yields and a strong solvatochromic effect, *Chem. Commun.*, 2023, **59**, 2923–2926.

38 A. Y. Baranov, S. O. Slavova, A. S. Berezin, S. K. Petrovskii, D. G. Samsonenko, I. Y. Bagryanskaya, V. P. Fedin, E. V. Grachova and A. V. Artem'ev, Controllable synthesis and luminescence behavior of tetrahedral $Au@Cu_4$ and $Au@Ag_4$ clusters supported by tris(2-pyridyl)phosphine, *Inorg. Chem.*, 2022, **61**, 10925–10933.

39 M. J. Calhorada, C. Ceamanos, O. Crespo, C. M. Gimeno, A. Laguna, C. Larraz, P. D. Vaz and M. D. Villacampa, Heteropolynuclear gold complexes with metallophilic interactions: modulation of the luminescent properties, *Inorg. Chem.*, 2022, **49**, 8255–8269.

40 V. J. Catalano, J. M. López-de-luzuriaga, M. Monge, M. E. Olmos and D. Pascual, Copper(I)-assisted red-shifted phosphorescence in Au(I)···Cu(I) heteropolynuclear complexes, *Dalton Trans.*, 2014, **43**, 16486–16497.

41 E. Hobbollahi, M. List, B. Hupp, F. Mohr, R. J. F. Berger, A. Steffen and U. Monkowius, Highly efficient cold-white light emission in a $[Au_2CuCl_2(P\cap N)_2]PF_6$ type salt, *Dalton Trans.*, 2017, **46**, 3438–3442.

42 Y. Yang, X.-L. Pei and Q.-M. Wang, Postclustering dynamic covalent modification for chirality control and chiral sensing, *J. Am. Chem. Soc.*, 2013, **135**, 16184–16191.

43 X.-L. Pei, Z.-J. Guan, Z.-A. Nan and Q.-M. Wang, Heterometallic coinage metal acetylenediide clusters showing tailored thermochromic luminescence, *Angew. Chem., Int. Ed.*, 2021, **60**, 14381–14384.

44 Z. Lei, Z.-J. Guan, X.-L. Pei, S.-F. Yuan, X.-K. Wan, J.-Y. Zhang and Q.-M. Wang, An atomically precise $Au_{10}Ag_2$ nanocluster with red–near-IR dual emission, *Chem. – Eur. J.*, 2016, **22**, 11156–11160.

45 H. Yang, Y. Wang, J. Lei, L. Shi, X. Wu, V. Mäkinen, S. Lin, Z. Tang, J. He, H. Häkkinen, L. Zheng and N. Zheng, Ligand-stabilized $Au_{13}Cu_x$ (x = 2, 4, 8) bimetallic nanoclusters: ligand engineering to control the exposure of metal sites, *J. Am. Chem. Soc.*, 2013, **135**, 9568–9571.

46 J.-H. Jia, J.-X. Liang, Z. Lei, Z.-X. Cao and Q.-M. Wang, A luminescent gold(I)–copper(I) cluster with unprecedented carbon-centered trigonal prismatic hexagold, *Chem. Commun.*, 2011, **47**, 4739–4741.

47 J.-H. Jia and Q.-M. Wang, Intensely luminescent gold(I)–silver(I) cluster with hypercoordinated carbon, *J. Am. Chem. Soc.*, 2009, **131**, 16634–16635.

48 Z. Lei, X.-L. Pei, Z.-J. Guan and Q.-M. Wang, Full protection of intensely luminescent gold(I)–silver(I) cluster by phosphine ligands and inorganic anions, *Angew. Chem., Int. Ed.*, 2017, **56**, 7117–7120.

49 A. Y. Baranov, E. A. Pritchina, A. S. Berezin, D. G. Samsonenko, V. P. Fedin, N. A. Belogorlova, N. P. Gritsan and A. V. Artem'ev, Beyond classical coordination chemistry: the first case of a triply bridging phosphine ligand, *Angew. Chem., Int. Ed.*, 2021, **60**, 12577–12584.

50 I. R. Dayanova, A. V. Shamsieva, I. D. Strelnik, T. P. Gerasimova, I. E. Kolesnikov, R. R. Fayzullin, D. R. Islamov, A. F. Saifina, E. I. Musina, E. Hey-Hawkins and A. A. Karasik, Assembly of heterometallic $AuICu_2I_2$ cores on the scaffold of NPPN-bridging cyclic bisphosphine, *Inorg. Chem.*, 2021, **60**, 5402–5411.

51 A. V. Artem'ev, A. Y. Baranov, A. S. Berezin, U. A. Lapteva, D. G. Samsonenko and I. Y. Bagryanskaya, Trigonal planar $Au@Ag_3$ clusters showing exceptionally fast and efficient phosphorescence in violet to deep-blue region, *Chem. – Eur. J.*, 2022, **28**, e202201563.

52 C. Kirst, J. Tietze, P. Mayer, H.-C. Böttcher and K. Karaghiosoff, Coinage metal complexes of bis(quinoline-2-ylmethyl)phenylphosphine-simple reactions can lead to unprecedented results, *ChemistryOpen*, 2022, **11**, e202100224.

53 A. Del Zotto, G. Nardin and P. Rigo, Copper(I), silver(I) and gold(I) complexes with the hybrid ligand 1-(diphenylphosphino)-2-(2-pyridyl)ethane (ppye). Variable-temperature nuclear magnetic resonance investigations and the crystal

structure of [Au(ppye-P)$_2$]PF$_6$, *J. Chem. Soc., Dalton Trans.*, 1995, 3343–3351.

54 F. Hung-Low and K. K. Klausmeyer, Silver coordination complexes of 2-(diphenylphosphinomethyl)pyridine and their bipyridine derivatives, *Inorg. Chim. Acta*, 2008, **361**, 1298–1310.

55 Z. Liu, P. I. Djurovich, M. T. Whited and M. E. Thompson, Cu_4I_4 clusters supported by P∧N-type ligands: new structures with tunable emission colors, *Inorg. Chem.*, 2012, **51**, 230–236.

56 P. Mayer, D. Fattakhova-Rohlfing, C. Kirst, F. Zoller, T. Bräuniger and K. Karaghiosoff, Investigation of structural changes of Cu(I) and Ag(I) complexes utilizing a flexible, yet sterically demanding multidentate phosphine oxide ligand, *Inorg. Chem.*, 2021, **60**, 2437–2445.

57 M. Frik, J. Jiménez, I. Gracia, L. R. Falvello, S. Abi-Habib, K. Suriel, T. R. Muth and M. Contel, Luminescent di- and polynuclear organometallic gold(I)–metal (Au_2, $\{Au_2Ag\}_n$ and $\{Au_2Cu\}_n$) compounds containing bidentate phosphanes as active antimicrobial agents, *Chem. – Eur. J.*, 2012, **18**, 3659–3674.

58 S. J. Berners-Price, R. J. Bowen, P. J. Harvey, P. C. Healy and G. A. Koutsantonis, Silver(I) nitrate adducts with bidentate 2-, 3- and 4-pyridyl phosphines. Solution ^{31}P and [^{31}P–^{109}Ag] NMR studies of 1:2 complexes and crystal structure of dimeric [{Ag(d2pype)(μ-d2pype)}$_2$][NO$_3$]$_2$·2CH$_2$Cl$_2$ [d2pype = 1,2-bis(di-2-pyridylphosphino)ethane, *J. Chem. Soc., Dalton Trans.*, 1998, 1743–1750.

59 A. S. Humphreys, A. Filipovska, S. J. Berners-Price, G. A. Koutsantonis, B. W. Skelton and A. H. White, Gold(I) chloride adducts of 1,3-bis(di-2-pyridylphosphino)propane: synthesis, structural studies and antitumour activity, *Dalton Trans.*, 2007, 4943–4950.

60 R. J. Bowen, M. Navarro, A.-M. J. Shearwood, P. C. Healy, B. W. Skelton, A. Filipovska and S. J. Berners-Price, 1 : 2 Adducts of copper(I) halides with 1,2-bis(di-2-pyridylphosphino)ethane: solid state and solution structural studies and antitumour activity, *Dalton Trans.*, 2009, 10861–10870.

61 S. J. Berners-Price, R. J. Bowen, T. W. Hambley and P. C. Healy, NMR and structural studies of gold(I) chloride adducts with bidentate 2-, 3- and 4-pyridyl phosphines, *J. Chem. Soc., Dalton Trans.*, 1999, 1337–1346.

62 I. D. Strelnik, V. V. Gurzhiy, V. V. Sizov, E. I. Musina, A. A. Karasik, S. P. Tunik and E. V. Grachova, A stimuli-responsive Au(I) complex based on an aminomethylphosphine template: synthesis, crystalline phases and luminescence properties, *CrystEngComm*, 2016, **18**, 7629–7635.

63 I. D. Strelnik, V. V. Sizov, V. V. Gurzhiy, A. S. Melnikov, I. E. Kolesnikov, E. I. Musina, A. A. Karasik and E. V. Grachova, Binuclear gold(I) phosphine alkynyl complexes templated on a flexible cyclic phosphine ligand: synthesis and some features of solid-state luminescence, *Inorg. Chem.*, 2020, **59**, 244–253.

64 N. A. Shamsutdinova, I. D. Strelnik, E. I. Musina, T. P. Gerasimova, S. A. Katsyuba, V. M. Babaev, D. B. Krivolapov, I. A. Litvinov, A. R. Mustafina, A. A. Karasik and O. G. Sinyashin, "Host–guest" binding of a luminescent dinuclear Au(I) complex based on cyclic diphosphine with organic substrates as a reason for luminescence tuneability, *New J. Chem.*, 2016, **40**, 9853–9861.

65 S. H. Lim, M. M. Olmstead and A. L. Balch, Molecular accordion: vapoluminescence and molecular flexibility in the orange and green luminescent crystals of the dimer, Au_2(μ-bis-(diphenylphosphino)ethane)$_2Br_2$, *J. Am. Chem. Soc.*, 2011, **133**, 10229–10238.

66 W. Yu, O. Fuhr and D. Fenske, Derivatives of bis(diphenylphosphino)maleic anhydride as ligands in polynuclear gold(I) complexes, *J. Cluster Sci.*, 2012, **23**, 753–766.

67 A. Bondi, van der Waals volumes and radii, *J. Phys. Chem.*, 1964, **68**, 441–451.

68 D. Li, X. Hong, C.-M. Che, W.-C. Lo and S.-M. Peng, Luminescent gold(I) acetylide complexes. Photophysical and photoredox properties and crystal structure of [{Au(C≡CPh)}$_2$(μ-Ph$_2$PCH$_2$CH$_2$PPh$_2$)], *J. Chem. Soc., Dalton Trans.*, 1993, 2929–2932.

69 J. Cámara, M. C. Blanco, A. Laguna, P. Naumov and M. C. Gimeno, A stable gold(I)–enyne species obtained by alkyne carboauration in a complex rearrangement, *Chem. Commun.*, 2017, **53**, 9202–9205.

70 N. Svahn, A. J. Moro, C. Roma-Rodrigues, R. Puttreddy, K. Rissanen, P. V. Baptista, A. R. Fernandes, J. C. Lima and L. Rodríguez, The important role of the nuclearity, rigidity, and solubility of phosphane ligands in the biological activity of gold(I) complexes, *Chem. – Eur. J.*, 2018, **24**, 14654–14667.

71 M. Osawa, S. Soma, M. Hoshino, Y. Tanaka and M. Akita, Photoluminescent properties and molecular structures of dinuclear gold(I) complexes with bridged diphosphine ligands: near-unity phosphorescence from ^{3}XMMCT/^{3}MC, *Dalton Trans.*, 2020, **49**, 15204–15212.

72 J. B. Foley, S. E. Gay, M. J. Vela, B. M. Foxman, A. E. Bruce and M. R. M. Bruce, Structure and photochemical isomerization of the dinuclear gold(I) halide bis(diphenylphosphanyl)ethylene complexes: correlation between quantum yield and aurophilicity, *Eur. J. Inorg. Chem.*, 2007, **2007**, 4946–4951.

73 N. Glebko, T. M. Dau, A. S. Melnikov, E. V. Grachova, I. V. Solovyev, A. Belyaev, A. J. Karttunen and I. O. Koshevoy, Luminescence thermochromism of gold(I) phosphane–iodide complexes: a rule or an exception?, *Chem. – Eur. J.*, 2018, **24**, 3021–3029.

74 I. O. Koshevoy, L. Koskinen, E. S. Smirnova, M. Haukka, T. A. Pakkanen, A. S. Melnikov and S. P. Tunik, Synthesis, structural characterization and luminescence studies of di- and trinuclear gold(I) alkynyl-phosphine complexes, *Z. Anorg. Allg. Chem.*, 2010, **636**, 795–802.

75 L. Rodríguez, M. Ferrer, R. Crehuet, J. Anglada and J. C. Lima, Correlation between photophysical parameters and gold–gold distances in gold(I) (4-pyridyl)ethynyl complexes, *Inorg. Chem.*, 2012, **51**, 7636–7641.

76 B.-C. Tzeng, W.-C. Lo, C.-M. Che and S.-M. Peng, Photophysical properties, crystal structure, and host–guest interaction of a luminescent tetranuclear gold(I)-phenylacetylide complex with a supramolecular phosphine ligand, *Chem. Commun.*, 1996, 181–182.

77 M. Pujadas and L. Rodríguez, Luminescent phosphine gold (I) alkynyl complexes. Highlights from 2010 to 2018, *Coord. Chem. Rev.*, 2020, **408**, 213179.

78 L. Chen, X. Chen, R. Ma, K. Lin, Q. Li, J.-P. Lang, C. Liu, K. Kato, L. Huang and X. Xing, Thermal enhancement of luminescence for negative thermal expansion in molecular materials, *J. Am. Chem. Soc.*, 2022, **144**, 13688–13695.

79 T. Wu, S. Jiang, P. N. Samanta, Y. Xie, J. Li, X. Wang, M. Devashis, X. Gu, Y. Wang, W. Huang, Q. Zhang, J. Leszczynski and D. Wu, Negative thermal quenching of photoluminescence in a copper–organic framework emitter, *Chem. Commun.*, 2020, **56**, 12057–12060.

80 M. Li, Z. Cheng, X. Wang, Z. Yu, M. Zhou, H. Miao, W. Zhaxi, W. Huang, X. Ma, Q. Chen, S. Jiang, Q. Zhang and D. Wu, Negative/zero thermal quenching of luminescence via electronic structural transition in copper–iodide cluster-based coordination networks, *J. Phys. Chem. Lett.*, 2021, **12**, 8237–8245.

81 R. Czerwieniec, M. J. Leitl, H. H. H. Homeier and H. Yersin, Cu(I) complexes – Thermally activated delayed fluorescence. Photophysical approach and material design, *Coord. Chem. Rev.*, 2016, **325**, 2–28.

82 A. Gusev, E. Braga, E. Zamnius, M. Kiskin, A. Ali, G. Baryshnikov and W. Linert, Mononuclear copper(I) complexes bearing a 3-phenyl-5-(pyridin-4-yl)-1,2,4-triazole ligand: synthesis, crystal structure, TADF-luminescence, and mechanochromic effects, *Dalton Trans.*, 2023, **52**, 14995–15008.

83 S.-Y. Tang, L. Song, Y.-F. Jia, W.-Z. Xu, Y.-X. Yang, L.-J. Sun, H.-Y. Shen and W.-X. Chai, Three heteroleptic copper(I) complexes with $[Cu(P\wedge P)N_2]^+$ structure and their fluorescence sensing for VOCs, *Appl. Organomet. Chem.*, 2023, **37**, e7242.

84 S. Cheng, Z. Chen, Y. Yin, Y. Sun and S. Liu, Progress in mechanochromic luminescence of gold(I) complexes, *Chin. Chem. Lett.*, 2021, **32**, 3718–3732.

85 Z.-Q. Dai, L. Song, J.-E. Chen, D.-F. Jin, H.-X. Jin, X.-L. Guo, H.-Y. Shen and W.-X. Chai, Smart-responsive luminescence and VOC sensing application of a copper(I) cluster with a novel $P_2CuI_2CuN_2$ core, *J. Mater. Chem. C*, 2025, **13**, 7234–7244.

86 J. Delafoulhouze, M. Cordier, J.-Y. Mevellec, F. Massuyeau, O. Hernandez, C. Latouche and S. Perruchas, Mechanoresponsive luminescence triggered by phase transition of a supercooled copper(I) complex, *Chem. Commun.*, 2024, **60**, 5278–5281.

87 Y.-Z. Huang, R. K. Gupta, G.-G. Luo, Q.-C. Zhang and D. Sun, Luminescence thermochromism in atomically precise silver clusters: a comprehensive review, *Coord. Chem. Rev.*, 2024, **499**, 215508.